Strain-controlled oxygen vacancy formation and ordering in $CaMnO_3$

Ulrich Aschauer,[1,*] Reto Pfenninger,[1] Sverre M. Selbach,[1,2] Tor Grande,[2] and Nicola A. Spaldin[1]
[1]*Materials Theory, ETH Zurich, Wolfgang-Pauli-Strasse 27, CH-8093 Zürich, Switzerland*
[2]*Department of Materials Science and Engineering, Norwegian University of Science and Technology, NO-7491 Trondheim, Norway*
(Received 1 April 2013; revised manuscript received 27 May 2013; published 19 August 2013)

We use first-principles calculations to investigate the stability of biaxially strained *Pnma* perovskite $CaMnO_3$ towards the formation of oxygen vacancies. Our motivation is provided by promising indications that novel material properties can be engineered by application of strain through coherent heteroepitaxy in thin films. While it is usually assumed that such epitaxial strain is accommodated primarily by changes in intrinsic lattice constants, point defect formation is also a likely strain-relaxation mechanism. Our first-principles calculations of oxygen vacancy defect formation energy indeed show a strong strain dependence: We find that tensile strain lowers the formation energy, consistent with the established chemical expansion concept that oxygen deficiency increases the molar volume in oxides. In addition, we find that strain differentiates the formation energy for different lattice sites, suggesting its use as a route to engineering vacancy ordering in epitaxial thin films.

DOI: 10.1103/PhysRevB.88.054111 PACS number(s): 68.55.Ln, 77.80.bn, 71.15.Mb

I. INTRODUCTION

Materials of the ABO_3 perovskite family and derived structures exhibit a large variety of functional properties which are of fundamental and technological interest. Intrinsic and extrinsic point defects, such as oxygen vacancies or cation nonstoichiometry, always exist in these materials and are in some cases desirable or even crucial for their properties. For example, oxygen vacancies enable ionic conductivity in high-temperature electrochemical devices such as oxygen sensors, solid oxide fuel cell (SOFC) cathodes, and mixed conducting membranes.[1,2] Deviations from ideal stoichiometry and charge balance are essential for introducing the carriers required for conventional conductivity or superconductivity, or carrier-mediated ferromagnetic ordering. The arrangement of defects can also be important, with reports of *ordered* oxygen vacancies inducing high-temperature superconductivity[3,4] and multiferroicity.[5] The electronic structure of interfaces in oxide heterostructures such as the formation of two-dimensional electron gases (2DEGs)[6] possibly relies on cation interdiffusion and will thus be critically affected by the concentration of cation vacancies required for cation migration. Point defects can also be detrimental, however, particularly if insulating behavior is desired, such as in ferroelectric or capacitor applications, or in achieving intrinsic antiferromagnetic ordering through superexchange.

In bulk perovskite oxides the presence of oxygen vacancies is well established to result in an expansion of the crystal lattice due to underbonding caused by the two extra electrons from the missing oxygen located in nonbonding orbitals.[7,8] This phenomenon, known as chemical expansion, is most pronounced for perovskites containing transition-metal ions that can adopt a variety of valence states and hence can readily accommodate the associated change in formal charge.[9] Prominent examples are acceptor doped $LaMnO_3$ and donor doped $SrTiO_3$,[10,11] where significant volume expansions are observed as a function of the oxygen partial pressure.

It has been demonstrated during the last decade that functional behavior in perovskites can be enabled or enhanced when they are prepared as thin films. For example, ferroelectricity has been reported in thin films of $SrTiO_3$, which is a quantum paraelectric in its bulk form, and enhanced polarization has been observed in thin films of ferroelectric $BaTiO_3$.[12,13] Reports of coupling magnetic and ferroelectric order parameters to yield thin-film magnetoelectric multiferroics[14,15] have spiked tremendous interest. The improved behavior is usually attributed to the biaxial epitaxial strain introduced when the film is grown coherently on a substrate with a different lattice constant. In turn, it is assumed that the change in the in-plane lattice constant associated with epitaxial strain is accommodated through structural distortions such as changing the internal bond lengths (top row of Fig. 1), or changing the angle or pattern of rotations and tilts of the oxygen octahedra (center row of Fig. 1).[16–18] Indeed, first-principles electronic-structure calculations within this approximation have proven successful in predicting and explaining many of the observed novel behaviors;[14,19,20] for a review see Ref. 18.

In addition to changes in internal bond lengths or octahedral rotations, another possible effect of the change in lattice parameter forced by coherent epitaxy is a change in the defect profile. Such a response is likely because both strain and point defects affect the molar volume and hence the Gibbs free energy resulting in strain dependent defect formation energies. The increase in volume associated with biaxial tensile strain is likely to increase the concentration of oxygen vacancies (Fig. 1, lower right panel). In the opposite direction, compressive strain should increase the concentration of cation vacancies (Fig. 1, lower left panel) due to the concomitant charge balancing oxidation of cations with smaller ionic radii at higher oxidation states. Coherent epitaxial strain could thus be used as a parameter to control point defect populations. Conversely, the spontaneous formation of oxygen vacancies could act as a route of chemistry mediated strain relaxation[10,21,22] and allow large lattice mismatches to be accommodated in heterostructures. We explore these possibilities here.

We choose the perovskite $CaMnO_3$ as our model compound for analyzing the strain dependence of the oxygen vacancy (V_O) formation reaction. $CaMnO_3$ forms in the widely adopted *Pnma* modification of the ideal perovskite structure (Fig. 2), and this tilt pattern has been shown to remain stable

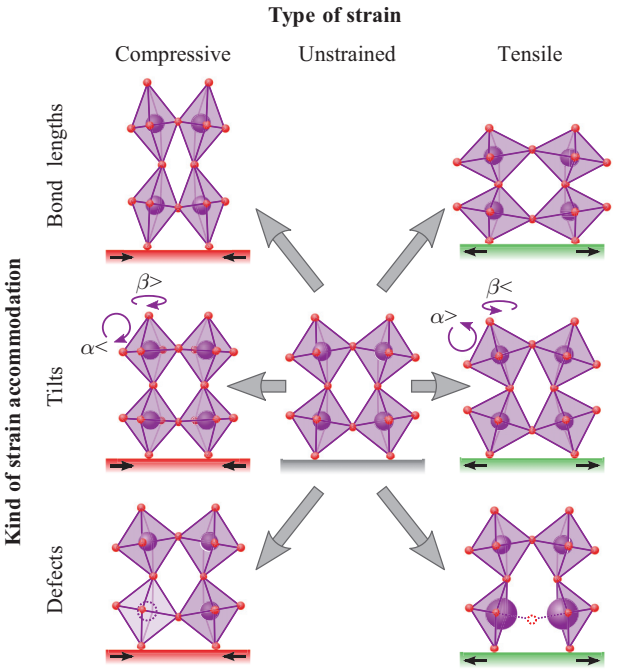

FIG. 1. (Color online) Schematic illustration of possible mechanisms for epitaxial strain accommodation in perovskites. Only B-site octahedra are shown, A-site cations being omitted for clarity. Top row: accommodation by bond-length changes; center row: accommodation by changes in octahedral tilt (α) and rotation (β) magnitudes; bottom row: accommodation by point defect formation. In the bottom right we illustrate the chemical expansion associated with oxygen vacancy formation, which is the subject of this work; the bottom left shows the "chemical contraction" caused by cation vacancy formation with concomitant oxidation of cations (Ref. 10).

throughout the entire range of likely experimentally accessible strains.[15,20,23] The oxygen vacancy has a charge of +2 relative to the perfect lattice, usually written as $V_O^{\bullet\bullet}$ in Kröger-Vink notation, but here V_O is used for simplicity. This relative charge of V_O has to be compensated by point defects with opposite charge to retain charge neutrality. The compensating point defect is Mn^{3+} on Mn^{4+} sites with a relative charge of -1, Mn'_{Mn} in Kröger-Vink notation. The chemical reaction that

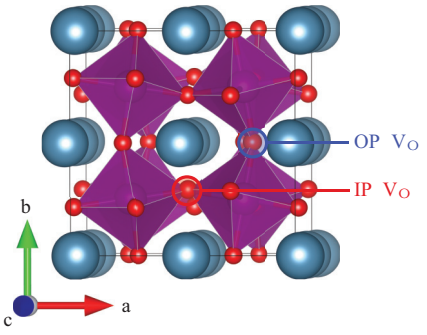

FIG. 2. (Color online) The *Pnma* crystal structure of bulk, unstrained $CaMnO_3$. The two inequivalent V_O positions, which are adjacent to Mn ions in the strained ac plane (IP) and perpendicular to it (OP) are indicated. Color code: Ca: blue; Mn: purple; O: red.

we study can be written as

$$2Mn^{4+} + O^{2-} \rightarrow 2Mn^{3+} + V_O + {}^1\!/_2 O_2(g) \qquad (1)$$

and has an experimental enthalpy of 1.89 ± 0.04 eV in bulk $CaMnO_3$.[24] Since high-spin Mn^{3+} (0.645 Å) is larger than Mn^{4+} (0.53 Å),[25] it is clear that reaction (1) should be accompanied by a considerable volume expansion, which indeed is supported by experiments.[26,27] Since volume increases (decreases) with tensile (compressive) strain, we expect the V_O formation energy to be sensitive to strain. In addition to this volume effect, strain may also affect the V_O formation energy through its effect on the electronic energy levels. The electrons from the loss of O_2 which reduce Mn^{4+} to Mn^{3+} occupy the e_g orbitals, the energies of which are strongly affected by the coordination geometry of the surrounding ions.

Our main finding is that, as expected, tensile strain lowers the oxygen vacancy formation energy in $CaMnO_3$. This shows that the material will respond to tensile strain not only by increasing its bond lengths and modifying its octahedral rotation angles, but also by reducing its oxygen stoichiometry by creation of oxygen vacancies. In addition, and perhaps unexpectedly, we find that strain modifies the oxygen vacancy formation energy of inequivalent oxygen sites markedly differently. This finding implies a possible strain control of oxygen vacancy ordering, which could enable new functionalities.[28,29]

II. COMPUTATIONAL DETAILS

Density functional theory (DFT) calculations were performed using the VASP code,[30–33] with the PBEsol functional[34] and wave functions expanded in plane waves up to a kinetic energy cutoff of 650 eV. The projector augmented wave (PAW)[35,36] method was used to describe electron-core interactions with Ca($3s, 3p, 4s$), Mn($3p, 3d, 4s$), and O($2s, 2p$) shells treated as valence electrons. The Hubbard U correction[37] was applied to Mn $3d$ electrons, using a U value of 3.0 eV, which was found to reproduce the experimentally determined density of states[38] and was recently shown to yield the correct stability of the different magnetic phases of $CaMnO_3$,[39] as well as the redox energetics of binary manganese oxides.[40] We used the ground-state G-type antiferromagnetic order in conjunction with a $2 \times 2 \times 2$ supercell of the five-atom perovskite unit cell. Reciprocal space integration was performed on a $4 \times 4 \times 4$ Γ-centered mesh. Structures were set up within the desired *Pnma* space group and subsequently relaxed until forces on the ions converged to below 10^{-5} eV/Å. In our calculations we strained $CaMnO_3$ in the plane of the equal a and c axes, while relaxing the b-axis length and all internal coordinates. It should be noted that the film can adopt additional orientations with respect to the substrate,[15] however as a proof of concept we limit ourselves to just one case. During calculations containing V_O the lattice parameters were kept fixed respectively at the strained $a = c$ and relaxed b lattice parameter, while relaxing only internal coordinates. The oxygen vacancy formation energy ΔE_{form} was computed from

$$\Delta E_{\text{form}}(\epsilon, \mu_O) = E_{\text{tot},V_O} - E_{\text{tot,stoi}} + \mu_O. \qquad (2)$$

Here ϵ and μ_O are the strain and the oxygen chemical potential respectively. $E_{\text{tot,stoi}}$ and E_{tot,V_O} denote the DFT total

energy of the stoichiometric simulation cell and that containing one oxygen vacancy respectively. Using this approach we determine the formation energy and hence the oxygen vacancy concentration as a function of imposed epitaxial strain. This can be thought of as the inverse of chemical expansion, where the volume (isotropic strain) changes due to the concentration of oxygen vacancies imposed by the environment. We chose this "inverse" approach as it is less susceptible to computational artefacts such as Pulay stresses.[41]

III. RESULTS AND DISCUSSION

A. Stoichiometric $CaMnO_3$

We first look at strain induced changes in the stoichiometric $CaMnO_3$ structure, characterized by the volume, lattice parameters, bond lengths, and octahedral rotation angles shown in Fig. 3. We notice first in Fig. 3(a) that strain leads to a net volume change in $CaMnO_3$, meaning that the material does not have a perfect Poisson ratio. This is also reflected in the lattice parameters shown in Fig. 3(b). While the a and c lattice parameters change linearly as a function of the imposed strain, the b lattice parameter expands more strongly in the compressive range than it shrinks in the tensile range. Its rate of change is however about a factor 2 smaller than required for constant volume, leading to the observed volume decrease with increasing compression.

As schematically shown in Fig. 1, in the stoichiometric structure, these changes in lattice parameter are accommodated by changes in bond lengths and octahedral rotation angles. Indeed in Figs. 3(c) and 3(d) we see that both the bond lengths and tilt angles change as a function of biaxial strain. The bond lengths are however relatively insensitive to strain (an order of magnitude smaller change than the lattice parameters, compare

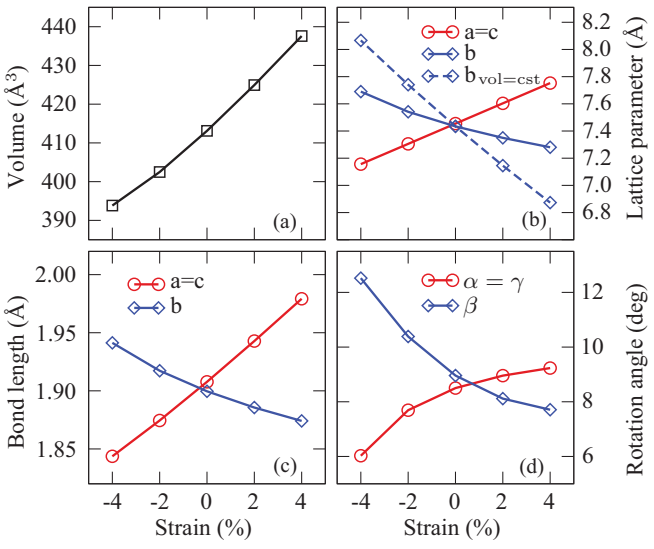

FIG. 3. (Color online) Evolution of structural properties with biaxial strain in stoichiometric $CaMnO_3$: (a) relaxed eight-formula-unit supercell volume (a material with an ideal Poisson ratio would have a constant volume with strain), (b) lattice parameters (the dashed line shows the b-axis parameter for a material with ideal poisson ratio), (c) Mn-O bond lengths, and (d) octahedral rotation angles (defined as angles between Cartesian axes and Mn-O bonds).

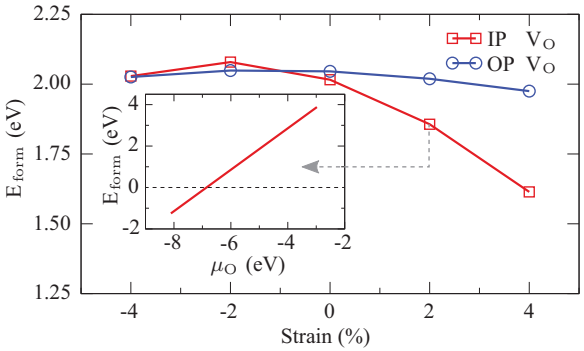

FIG. 4. (Color online) V_O formation energies for the two inequivalent V_O positions in the *Pnma* tilted $CaMnO_3$ structure at an oxygen chemical potential of -5 eV, corresponding to typical growth conditions under air. The inset shows the formation energy of the IP V_O at 2% tensile strain as a function of the oxygen chemical potential. The OP V_O very closely tracks this curve and is omitted for clarity.

Fig. 3(b) to Fig. 3(c)), meaning that for stoichiometric *Pnma* $CaMnO_3$ biaxial strain is primarily accommodated by altering the octahedral tilt angles, Fig. 3(d). As expected, the octahedral tilt angles increase with compression of the respective axis, and decrease when the axis becomes longer.

B. Tensile strain

In the orthorhombic $CaMnO_3$ structure there are two inequivalent oxygen positions as shown in Fig. 2. We label these IP and OP, corresponding to the broken Mn-O bonds lying in or out of the plane of epitaxial strain respectively, but note that the sites are already inequivalent in the unstrained *Pnma* structure. In Fig. 4 we show our calculated formation energies for these two oxygen vacancies as a function of the applied strain at an oxygen chemical potential of -5 eV, corresponding to typical growth conditions under air. It should be noted that the limited size of the simulation cell results in a fairly high vacancy concentration and could in principle lead to artificially increased formation energies. The good agreement with respect to the experimental formation energy of 1.89 ± 0.04 eV (Ref. 24) under similar conditions however leads us to believe that this effect should be small. Moreover, as we will show below, vacancy concentrations such as those simulated are in fact experimentally accessible at typical growth temperatures and under reducing conditions. In the inset in Fig. 4 we also show the V_O formation energy in the 2% tensile strained structure as a function of the oxygen chemical potential throughout the whole range of $CaMnO_3$ thermodynamic stability evaluated by computing the Ca-Mn-O ternary phase diagram.[42] As is well known, the oxygen chemical potential strongly affects the absolute value of the formation energy and hence the equilibrium oxygen vacancy concentration.

1. Change in stoichiometry

As expected from the known chemical expansion caused by oxygen vacancies, we find that tensile strain lowers the formation energy for oxygen vacancies in $CaMnO_3$. The formation energy decreases considerably by ~0.4 eV

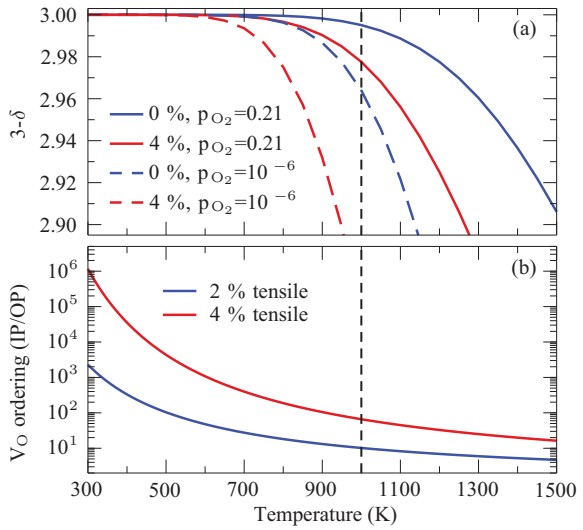

FIG. 5. (Color online) (a) Modelled oxygen stoichiometry of $CaMnO_{3-\delta}$ at 0% and 4% tensile strain and oxygen partial pressures (p_{O_2}) corresponding to air (0.21) and N_2 (10^{-6}) atmospheres respectively. The 3-δ curves are calculated from Eq. (3), see text for explanation. (b) Temperature-dependent V_O ordering expressed as the ratio of IP/OP (Fig. 2) for +2% and +4% tensile strain (Fig. 4). The typical growth temperature of 1000 K is indicated by the vertical dashed line.

corresponding to ~20% of the bulk value for formation of the IP vacancy at 4% strain.

In Fig. 5(a) we show the calculated equilibrium change in stoichiometry as a function of temperature for tensile strain values of 0 and 4% and oxygen partial pressures corresponding to growth in air (0.21) and under nitrogen (10^{-6}). The absolute oxygen stoichiometry 3-δ was estimated from reaction (1), the equilibrium constant of which can be written as[43]

$$K = \frac{[Mn^{3+}]^2[V_O]p_{O_2}^{1/2}}{[Mn^{4+}]^2[O^{2-}]} = \exp\left(-\frac{\Delta G_f}{k_B T}\right). \quad (3)$$

Here G_f is the Gibbs energy of reaction (1). From reaction (1) and charge neutrality we get $[V_O] = \delta$, $[Mn^{3+}] = 2\delta$, $[Mn^{4+}] = 1\text{-}2\delta$, and $[O^{2-}] = 3\text{-}\delta$. Equation (3) was solved for δ using $\Delta G_f = \Delta H_f - T\Delta S$ where ΔH_f is the enthalpy of oxygen vacancy formation and ΔS the entropy of reaction (1), respectively, where the latter is 95 J K^{-1} mol^{-1} taken from Ref. 43.

At a typical growth temperature of 1000 K (indicated by the vertical dashed line in Fig. 5), tensile strain of 4% reduces the equilibrium oxygen stoichiometry from 2.995 to 2.978 in air and from 2.964 to 2.859 in N_2 atmosphere ($p_{O_2} = 10^{-6}$ atm.), as illustrated in Fig. 5. The oxygen stoichiometry of the supercell used in our calculations is $3 - \delta = 2.875$ for comparison. A reduction of 0.4 eV of the V_O formation energy has an impact on δ equivalent to raising the temperature 150–200 K, and will drastically alter the equilibrium oxygen content.

2. *Vacancy ordering*

While both vacancy types lower their formation energy, we find that the energy lowering is stronger for the IP vacancy than for the OP, consistent with the fact that tensile strain expands the in-plane lattice parameter and leads to a slight contraction of the out-of-plane dimensions [see Fig. 3(b)], however still with a net increase in volume as shown in Fig. 3(a). This suggests that, in addition to tuning the oxygen vacancy formation energy, tensile biaxial strain could be used to influence vacancy site preference and thus induce vacancy ordering.

In Fig. 5(b) we show our calculated equilibrium ratio of IP to OP V_O as a function of temperature for tensile strain values of 2% and 4%. The ratio of IP to OP vacancies under tensile strain was calculated from the shift in formation energies shown in Fig. 4. Under +4% tensile strain, for example, the IP V_O formation energy is 0.36 eV lower than that of the OP V_O. At the typical growth temperature of 1000 K (Ref. 44) (indicated by the vertical dashed line in Fig. 5) this energy difference corresponds to an equilibrium ratio of IP to OP V_O = ~73. However, oxygen vacancies can remain mobile to much lower temperatures.[1,2,45] Equilibrium vacancy concentrations can thus be reached at significantly lower temperatures, especially in thin films where the diffusion distances are short.[10] At 300 K the equilibrium ratio of IP to OP vacancies is more than 10^6 [see Fig. 5(b)], demonstrating the possibility of engineering oxygen vacancy ordering by epitaxial strain. Oxygen vacancy ordering induced by epitaxial strain modification of the vacancy formation energy can in principle be applied to *any* oxide with nonequivalent oxygen sites. This can pave the way towards new interface functionalities arising from orbital ordering [Fig. 6(d)], localized electric dipoles/fields,[28] or enhanced interface electronic, ionic, or mixed conductivity.

C. Compressive strain

In spite of the fact that the volume of the cell decreases monotonically from tensile to compressive strain as shown in Fig. 3(a), we find a negligible change in the energy of formation of either vacancy on compressive strain. While our findings for tensile strain are consistent with the simple arguments based on changes in Mn ion valence and volume presented in the Introduction, the compressive-strain response is fundamentally different. Next we analyze the changes that strain induces in the electronic structure to understand the origin of this behavior.

In Fig. 6(a) we show our calculated electronic density of states (DOS) for unstrained $CaMnO_3$ with one out of 24 O atoms missing. We see that IP V_O formation produces an extra peak within the band gap of the density of states. The OP V_O produces a peak at nearly the same position and has hence been omitted for clarity. The IP V_O peak accommodates the two charge compensating electrons, which are primarily located in the formerly unoccupied z^2-type orbitals of the two Mn atoms adjacent to the oxygen vacancy, as shown in the calculated charge density in Fig. 6(d). Localization of these electrons is a result of the removal of the antibonding σ^* overlap between the Mn e_g and the O p orbitals along the axis of the broken bond, which lowers the energies of these e_g orbitals.

We also observe that both vacancies will cause an upward shift of about ~0.1 eV of the valence band edge, which consists of Mn t_{2g} orbitals. For the IP structure the increase stems from the xy and xz orbitals, whereas in the OP structure the xy and

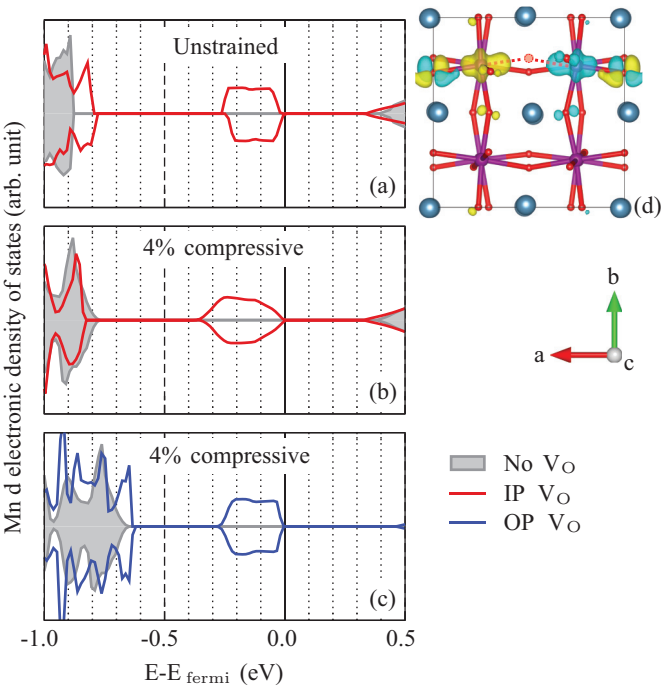

FIG. 6. (Color online) Mn d partial density of states shown for (a) the unstrained IP V_O case, (b) the IP V_O at 4% compressive strain, and (c) the OP V_O at 4% compressive strain. The DOS of the stoichiometric material is shown in grey for the corresponding strain. The energy scales of the stoichiometric DOS have been aligned with respect to the defective DOS at a Mn p core state about 50 eV below the Fermi energy. The origin in energy is set at the Fermi energy of the defective cell. Panel (d) shows the charge density associated with the occupied e_g states upon IP V_O formation. The dashed red lines and circle indicate the bonds and position of the missing O atom. Yellow and light blue isosurfaces at 8×10^{-3} eÅ^{-3} show the up and down spin density respectively. Color code: Ca: blue; Mn: purple, O: red.

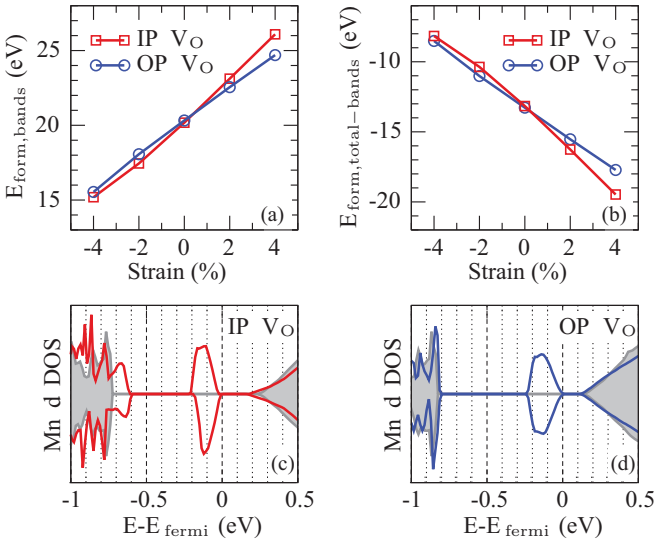

FIG. 7. (Color online) The total formation energy shown in Fig. 4 decomposed into contributions from (a) the band energy and (b) the remaining interactions. Panels (c) and (d) show the Mn d partial density of states at 4% tensile strain for the IP and OP V_O respectively compared to the stoichiometric case in grey. The energy scales are aligned as in Fig. 6.

yz orbitals move up in energy. This reflects the loss in Mn-O π bonding overlap with the bond broken by IP V_O formation lying along the a (x) axis, whereas that broken by OP V_O lies along the b (y) axis.

In Figs. 6(b) and 6(c) we look at the changes in band edge and gap state in the DOS of the IP and OP structure compared to the stoichiometric case. We can see that the valence band edge for the IP V_O is lowered by ∼0.05 eV, whereas for the OP V_O it is raised by an equal amount. We can again rationalize these effects in terms of structural changes. In the stoichiometric and IP case, the valence band edge consists primarily of xz orbitals lying in the compressed plane. Creation of an V_O in this plane can to some extent counteract the increase in antibonding overlap induced by compression and hence lead to a slight net lowering of the band-edge energy in the IP case. This is not the case for the OP V_O, for which moreover the xy and yz orbitals increase in energy due to loss of Mn-O bonding overlap, resulting in the observed net upwards shift.

The opposite trend is observed for the gap state, which is lowered in energy by ∼0.1 eV for the OP case, whereas in the IP case we observe a broadening with the lower edge dropping by ∼0.05 eV and the upper edge remaining more or less constant. The downwards shift of the OP gap state is due to decreased σ^* overlap since the broken Mn-O bonds lie along the stretched b axis. Conversely the broadening for the IP case stems from an increase of this overlap due to compression of the Mn-O bonds lying in the compressively strained plane. In the compressive regime we thus have counterbalancing effects, leading to very similar formation energies for the two vacancies, which are moreover almost independent of strain.

The above results indicate that crystal-field effects dominate changes in V_O formation energies under compression in contrast to the tensile case where we saw previously that chemical expansion dominates the behavior. The difference between the compressive and tensile cases can be further assessed by a decomposition of the V_O formation energy into its components. In Fig. 7 we see that in the tensile regime the band energy related part [Fig. 7(a)] alone would in fact predict E_{form} to increase under tensile strain and the OP V_O to be lower in energy than the IP V_O. In order to recover the observation in Fig. 4 that E_{form} decreases under tensile strain and that the IP V_O is more stable, the remaining—mainly electrostatic—interactions [Fig. 7(b)] have to dominate in the tensile range. In Figs. 7(c) and 7(d) we show the calculated partial density of states for the tensile strained case with IP and OP V_O respectively. We see that for the OP case there is almost no change in energy levels under tensile strain whereas for the IP case the upwards shift of the valence band is compensated by the downwards shift of the defect state, resulting in both cases in no net change of the band energy. The marked difference between IP and OP under tension is a result of the drastic reduction in repulsive electron-electron interaction due to stretching of the broken bond axis.

In our calculations relaxation of the internal coordinates allowed both octahedral rotation angles and bond lengths to vary as a function of strain. As mentioned earlier (Fig. 3), changes in octahedral rotation angles account for a large part of strain accommodation in the *Pnma* structure. Therefore

crystal-field effects due to bond-length changes should be rather weak. In order to assess the limit of strong crystal-field effects, when no changes in tilt pattern exist, we have performed the same analysis on the ideal cubic structure. Under tensile strain both vacancies show a similar although less marked behavior than in the *Pnma* structure. In the compressive range however we find the OP V_O formation energy to continuously increase whereas the IP V_O shows a marked decrease. This is the result of a pronounced broadening of the e_g gap states in the cubic structure as the strain is accommodated by changes in bond length (overlap) only. These observations confirm again that under compression crystal-field effects dominate whereas electrostatics are at the origin of the observed behavior under tensile strain.

IV. SUMMARY AND CONCLUSIONS

In the present work we have investigated how the oxygen vacancy formation energy is modified by biaxial strain from 4% compressive to 4% tensile strain. Our DFT calculations show that oxygen vacancy energetics are strongly modified by strain, particularly by tensile strain which was found to favor the formation of oxygen vacancies. Compared to the unstrained material, the formation energy of oxygen vacancies is reduced by up to 0.4 eV under 4% tensile strain, significantly reducing the equilibrium oxygen content in films under tensile strain. The origin of this reduction is mainly electrostatic, as tensile strain reduces the electron-electron repulsion along the broken Mn-O-Mn bond axis. It thus follows that $CaMnO_3$ can accommodate strain by increasing its concentration of oxygen vacancies.[10,21,46]

Compressive strain on the other hand was found to affect Mn *d* levels in a more subtle way with nearly no net effect on oxygen vacancy formation energies. Although not explicitly treated in this work, we expect the cation vacancy concentration in oxygen hyperstoichiometric perovskites, like $LaMnO_{3+\delta}$, to be correspondingly sensitive to compressive epitaxial strain.[10] In such materials the hyperstoichiometry is a result not of oxygen excess but cation deficiency.

This stabilization of oxygen vacancies by tensile strain is the reverse effect of the well established chemical expansion phenomenon where oxygen vacancies induce a unit-cell expansion.[7,8] Our findings have profound implications for the properties, growth, and thermal annealing of oxide thin films under tensile strain. Epitaxial strain, like temperature and partial pressure of oxygen (p_{O_2}), is a thermodynamic variable affecting the equilibrium oxygen stoichiometry.

The formation of oxygen vacancies must be charge compensated, either by reducing the formal oxidation state of cations (e.g., Mn^{4+} to Mn^{3+} in the present work) or more unfavorably by donating electrons into the high-energy conduction band [e.g., $LaAlO_3$ (Ref. 42)]. The formation of oxygen vacancies is therefore likely to be enhanced by tensile strain in *any* oxide with transition-metal cations with multiple oxidation states such as Mn, Fe, Co, Ni, or even Cu. The coupling between strain and oxygen vacancy formation energy is moreover expected to be most pronounced in materials containing transition-metal cations with localized *d* electrons.[47–49]

Our calculations also show that tensile strain affects the formation energy of the two kinds of nonequivalent oxygen vacancies in $CaMnO_3$ with *Pnma* perovskite structure in a markedly different way. Under 4% tensile strain the formation energy of oxygen vacancies on the in-plane site is 0.36 eV lower than on the out-of-plane site. Depending on the temperature, this large energy difference may result in orders of magnitude differences in vacancy concentrations on the two sites, and paves the way for tensile-strain-induced oxygen vacancy ordering. This possibility of engineering epitaxial heterostructures with oxygen vacancy ordering should apply to *any* oxide with nonequivalent oxygen sites.

ACKNOWLEDGMENTS

This work was supported financially by the ETH Zürich and by the ERC Advanced Grant program, No. 291151.

*uli.aschauer@mat.ethz.ch

[1]H. J. M. Bouwmeester, Catal. Today **82**, 141 (2003).
[2]J. Fleig, Annu. Rev. Mater. Res. **33**, 361 (2003).
[3]A. Ourmazd and J. C. H. Spence, Nature (London) **329**, 425 (1987).
[4]D. J. Werder, C. H. Chen, R. J. Cava, and B. Batlogg, Phys. Rev. B **38**, 5130 (1988).
[5]X. K. Wei, T. Zou, F. Wang, Q. H. Zhang, Y. Sun, L. Gu, A. Hirata, M. W. Chen, Y. Yao, C. Q. Jin, and R. C. Yu, J. Appl. Phys. **111**, 073904 (2012).
[6]J. Mannhart and D. G. Schlom, Science **327**, 1607 (2010).
[7]S. B. Adler, J. Am. Ceram. Soc. **84**, 2117 (2001).
[8]H. Ullmann and N. Trofimenko, J. Alloys Compd. **316**, 153 (2001).
[9]D. Marrocchelli, S. R. Bishop, H. L. Tuller, G. W. Watson, and B. Yildiz, Phys. Chem. Chem. Phys. **14**, 12070 (2012).
[10]T. Grande, J. R. Tolchard, and S. M. Selbach, Chem. Mater. **24**, 338 (2012).
[11]R. Moos and K. H. Hardtl, J. Am. Ceram. Soc. **80**, 2549 (1997).
[12]J. H. Haeni, P. Irvin, W. Chang, R. Uecker, P. Reiche, Y. L. Li, S. Choudhury, W. Tian, M. E. Hawley, B. Craigo, A. K. Tagantsev, X. Q. Pan, S. K. Streiffer, L. Q. Chen, S. W. Kirchoefer, J. Levy, and D. G. Schlom, Nature (London) **430**, 758 (2004).
[13]K. J. Choi, M. Biegalski, Y. L. Li, A. Sharan, J. Schubert, R. Uecker, P. Reiche, Y. B. Chen, X. Q. Pan, V. Gopalan, L. Q. Chen, D. G. Schlom, and C. B. Eom, Science **306**, 1005 (2004).
[14]J. H. Lee and K. M. Rabe, Phys. Rev. Lett. **104**, 207204 (2010).
[15]T. Günter, E. Bousquet, A. David, P. Boullay, P. Ghosez, W. Prellier, and M. Fiebig, Phys. Rev. B **85**, 214120 (2012).
[16]H. D. Megaw and C. N. W. Darlington, Acta Crystallogr., Sect. A **31**, 161 (1975).
[17]N. W. Thomas, Acta Crystallogr., Sect. B **52**, 939 (1996).
[18]J. M. Rondinelli and N. A. Spaldin, Adv. Mater. **23**, 3363 (2011).
[19]C. J. Fennie and K. M. Rabe, Phys. Rev. Lett. **97**, 267602 (2006).
[20]S. Bhattacharjee, E. Bousquet, and P. Ghosez, Phys. Rev. Lett. **102**, 117602 (2009).

[21]S. M. Selbach, T. Tybell, M.-A. Einarsrud, and T. Grande, Appl. Phys. Lett. **98**, 091912 (2011).
[22]G. J. la O, S.-J. Ahn, E. Crumlin, Y. Orikasa, M. D. Biegalski, H. M. Christen, and Y. Shao-Horn, Angew. Chem. Int. Ed. **49**, 5344 (2010).
[23]E. Bousquet and N. A. Spaldin, Phys. Rev. Lett. **107**, 197603 (2011).
[24]L. Rørmark, A. B. Mørch, K. Wiik, S. Stølen, and T. Grande, Chem. Mater. **13**, 4005 (2001).
[25]R. D. Shannon, Acta Crystallogr., Sect. A **32**, 751 (1976).
[26]X. Chen, J. Yu, and S. B. Adler, Chem. Mater. **17**, 4537 (2005).
[27]Z. Zeng, M. Greenblatt, and M. Croft, Phys. Rev. B **59**, 8784 (1999).
[28]A. Y. Borisevich, A. R. Lupini, J. He, E. A. Eliseev, A. N. Morozovska, G. S. Svechnikov, P. Yu, Y.-H. Chu, R. Ramesh, S. T. Pantelides, S. V. Kalinin, S. J. Pennycook, Phys. Rev. B **86**, 140102 (2012).
[29]S. V. Kalinin, A. Borisevich, and D. Fong, ACS Nano **6**, 10423 (2012).
[30]G. Kresse and J. Hafner, Phys. Rev. B **47**, 558 (1993).
[31]G. Kresse and J. Hafner, Phys. Rev. B **49**, 14251 (1994).
[32]G. Kresse and J. Furthmuller, Comput. Mater. Sci. **6**, 15 (1996).
[33]G. Kresse and J. Furthmuller, Phys. Rev. B **54**, 11169 (1996).
[34]J. P. Perdew, A. Ruzsinszky, G. I. Csonka, O. A. Vydrov, G. E. Scuseria, L. A. Constantin, X. Zhou, and K. Burke, Phys. Rev. Lett. **100**, 136406 (2008).
[35]P. E. Blöchl, Phys. Rev. B **50**, 17953 (1994).
[36]G. Kresse and D. Joubert, Phys. Rev. B **59**, 1758 (1999).
[37]V. I. Anisimov, J. Zaanen, and O. K. Andersen, Phys. Rev. B **44**, 943 (1991).
[38]J. H. Jung, K. H. Kim, D. J. Eom, T. W. Noh, E. J. Choi, J. Yu, Y. S. Kwon, and Y. Chung, Phys. Rev. B **55**, 15489 (1997).
[39]J. Hong, A. Stroppa, J. Íñiguez, S. Picozzi, and D. Vanderbilt, Phys. Rev. B **85**, 054417 (2012).
[40]L. Wang, T. Maxisch, and G. Ceder, Phys. Rev. B **73**, 195107 (2006).
[41]G. P. Francis and M. C. Payne, J. Phys.: Condens. Matter **2**, 4395 (1990).
[42]X. Luo, B. Wang, and Y. Zheng, Phys. Rev. B **80**, 104115 (2009).
[43]E. Bakken, J. Boerio-Goates, T. Grande, B. Hovde, T. Norby, L. Rørmark, R. Stevens, and S. Stølen, Solid State Ionics **176**, 2261 (2005).
[44]R. K. Zheng, H. U. Habermeier, H. L. W. Chan, C. L. Choy, and H. S. Luo, Phys. Rev. B **81**, 104427 (2010).
[45]X. Chen and T. Grande, Chem. Mater. **25**, 927 (2013).
[46]S. Venkatesan, M. Döblinger, C. Daumont, B. Kooi, B. Noheda, J. T. M. De Hosson, and C. Scheu, Appl. Phys. Lett. **99**, 222902 (2011).
[47]H. Jalili, J. W. Han, Y. Kuru, Z. Cai, and B. Yildiz, J. Phys. Chem. Lett. **2**, 801 (2011).
[48]W. Donner, C. Chen, M. Liu, A. J. Jacobson, Y.-L. Lee, M. Gadre, and D. Morgan, Chem. Mater. **23**, 984 (2011).
[49]A. Kushima, S. Yip, and B. Yildiz, Phys. Rev. B **82**, 115435 (2010).